Microfluid Nanofluid (2012) 12:65–73
DOI 10.1007/s10404-011-0849-7

RESEARCH PAPER

On-chip manipulation of nonmagnetic particles in paramagnetic solutions using embedded permanent magnets

Junjie Zhu · Litao Liang · Xiangchun Xuan

Received: 30 May 2011 / Accepted: 7 July 2011 / Published online: 20 July 2011

Abstract This study develops a method for embedding permanent magnets into poly(dimethylsiloxane) (PDMS)-based microfluidic chips. Magnets can be brought very close to the planar microchannels for enhanced magnetic field and field gradients, which enables on-chip continuous-flow manipulation of nonmagnetic particles in typical paramagnetic solutions. We performed a systematic study of the transport of polystyrene particles suspended in manganese (II) chloride ($MnCl_2$) solutions through a rectangular microchannel. Owing to their smaller magnetization than the suspending fluid, particles experience negative magnetophoresis and are deflected away from the magnet. The effects of particle position (relative to the magnet), particle size, $MnCl_2$ salt concentration, and fluid flow velocity on the horizontal magnetophoretic deflection are examined using a combined experimental and theoretical approach. The experimental results agree quantitatively with the predictions of an analytical model. The demonstrated nonmagnetic particle deflection may be used with the potential to focus and sort cells in lab-on-a-chip for bio-applications.

Keywords Microfluidics · Magnetophoresis · Nonmagnetic particle · Paramagnetic solution · Lab on a chip

1 Introduction

Magnetophoresis is a simple, efficient, and low-cost technique for particle manipulation in microfluidic devices (Pamme 2006; Gijs et al. 2010). It refers to the induced motion of particles in a non-uniform magnetic field (Jones 1995). Analogous to dielectrophoresis (Pohl 1978), magnetophoresis can be either positive or negative depending on whether the particle is more or less magnetizable than the suspending medium (Kirby 2010). Magnetic particles suspended in nonmagnetic solutions experience *positive* magnetophoresis and are directed along the magnetic field gradient toward a magnet (Pamme and Manz 2004; Gijs 2004; Pamme and Wilhelm 2006). On the contrary, nonmagnetic particles suspended in magnetic solutions undertake *negative* magnetophoresis and are pushed away from a magnet (Rosensweig 1985; Friedman and Yellen 2005). The former phenomenon has been widely employed to isolate and sort cells or biomolecules in microfluidic devices by selectively labeling the target ones with functionalized magnetic beads (Liu et al. 2009; Ando et al. 2010) or by utilizing their intrinsic paramagnetic feature (Han and Frazier 2006; Jung et al. 2010).

Ferrofluids (Rosensweig 1987; Erb and Yellen 2009) and paramagnetic salts (Suwa and Watarai 2011) are the magnetic solutions frequently employed to manipulate nonmagnetic particles that cover the majority of the synthetic and biological particles. As no magnetic tagging is needed, this negative magnetophoresis-based method can greatly facilitate the sample preparation and post-analysis, both of which are critical steps in lab on a chip for bio-applications. Ferrofluids have been demonstrated to pattern (Yellen et al. 2003, 2005; Yellen and Friedman 2004; Halverson et al. 2006), assemble (Feinstein and Prentiss 2006; Erb et al. 2009; Krebs et al. 2009; Li and Yellen 2010), concentrate (Fateen 2002; Erb and Yellen 2008; Annavarapu 2010), deflect (Sharpe 2004; Zhu et al. 2011), and separate (Kose et al. 2009; Zhu et al. 2010) particles with various sizes. They are, however, opaque liquids, and

J. Zhu · L. Liang · X. Xuan (✉)
Department of Mechanical Engineering, Clemson University, Clemson, SC 29634-0921, USA
e-mail: xcxuan@clemson.edu

so fluorescent staining is usually necessary in order to visualize the suspending particles.

In contrast, paramagnetic salts such as manganese(II) chloride ($MnCl_2$) and gadolinium(III) chloride ($GdCl_3$) solutions are transparent, which is beneficial to particle handling. However, their magnetic susceptibility is usually much smaller than that of ferrofluids (Mirica et al. 2009). Therefore, the salt concentration must be kept high in order to generate decent particle magnetophoresis, which makes the paramagnetic solution non-biocompatible (Rodriguez-Villarreal et al. 2011). Alternatively, strong magnet(s) [e.g., a superconducting magnet (Tarn et al. 2009)] must be employed to provide large magnetic fields. Another way is to bring magnet(s) very close to the microchannel that contains the particle suspension or even in contact with the suspension itself (Winkleman et al. 2004), so that the large magnetic field gradients can be achieved. Pamme's group (Peyman et al. 2009; Tarn et al. 2009; Rodriguez-Villarreal et al. 2011) and Watarai's group (Watarai and Namba 2001, 2002; Watarai et al. 2004) have each demonstrated continuous-flow control of particles and cells in paramagnetic solutions by the use of two closely facing magnets around a capillary. In addition, Park's group (Kang et al. 2008; Hahn and Park 2011) used an on-chip Nickel microstructure near the microchannel to locally enhance both the magnetic field and the field gradients for particle separation in paramagnetic buffers.

We develop herein a method to place permanent magnets to within 300-μm distance of an on-chip planar microchannel by embedding them into poly(dimethylsiloxane) (PDMS) directly. This enables the continuous-flow manipulation of nonmagnetic particles in typical paramagnetic solutions. To demonstrate this, we investigate the negative magnetophoretic deflection of polystyrene particles in $MnCl_2$ solutions through a rectangular microchannel. We also develop an analytical model to understand the observed particle motion, which is validated by the acquired experimental results. This model is believed to be applicable to previous studies on particle magnetophoresis in paramagnetic solutions.

2 Experiment

2.1 Device fabrication

Figure 1 shows a picture of the microfluidic device used in our experiment. The straight microchannel (filled with a green food dye for clarity) is 2-cm long, 200-μm wide and 25-μm deep. It was fabricated using a modified soft lithography method in order to embed permanent magnets into PDMS. Prior to the dispense of liquid PDMS over the channel master (Zhu et al. 2009), two stacked neodymium (NdFeB) permanent magnets (B221, K&J Magnetics, Inc.) were positioned 260 μm away from the edge of the microchannel. They were fixed to the substrate of the master by another permanent magnet (B421, K&J Magnetics, Inc.) from underneath the petri dish that held the master. These steps were performed under the microscope for a precise control. After the regular curing step, the magnet underneath the petri dish was removed, and the cured PDMS was carved out and bonded to a glass slide forming the microfluidic chip. A post-bonding baking was found to enhance the sealing quality of the microchannel. The embedded magnets each has a dimension of $1/8'' \times 1/8'' \times 1/16''$ (thick), and is magnetized through the thickness (i.e., z direction) that is perpendicular to the flow direction as seen in Fig. 1.

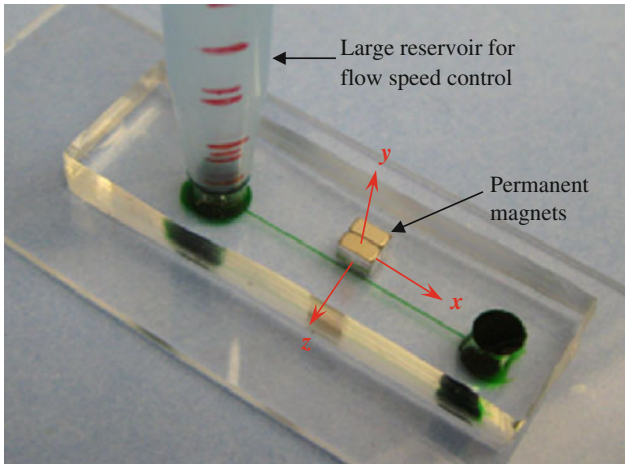

Fig. 1 Picture of the microfluidic chip with permanent magnets embedded in PDMS. The coordinate system, based on which the magnetic field and field gradients are determined, originates from the center of the permanent magnet whose magnetization direction is in line with the z coordinate

2.2 Preparation of particle suspensions

Manganese (II) chloride ($MnCl_2$) crystal was purchased from Fisher Scientific. It was dissolved in pure water to a concentration of 2 M, which was then stored in refrigerator for later uses. Prior to experiments, the stored $MnCl_2$ solution was diluted to 1 M, 200 mM, or 40 mM using pure water. Polystyrene particles of 5, 10, and 15 μm in diameters were obtained from Sigma-Aldrich. They are all originally packed as 10% solids in water with the size non-uniformity being less than 2%. Each type of these non-magnetic microparticles was re-suspended in a $MnCl_2$ solution (at one of the above-mentioned concentrations) to a final number density of about 1×10^6 particles/ml.

2.3 Particle manipulation and visualization

The particle suspensions in $MnCl_2$ solutions were driven through the microchannel by the liquid height difference in the upstream and downstream reservoirs. During experiment, the solution in the downstream reservoir was vacated. The liquid height in the upstream reservoir was varied to achieve different flow speeds, which were first estimated through theoretical calculations and then verified via experimental tracking of individual particles. Particle motion was visualized and recorded using an inverted microscope (Nikon Eclipse TE2000U, Nikon Instruments, Lewisville, TX) equipped with a CCD camera (Nikon DS-Qi1Mc). The obtained images were then processed using the Nikon imaging software (NIS-Elements AR 2.30).

3 Theory

3.1 Magnetic field-induced particle deflection

The magnetic force, $\mathbf{F}_m$, on a particle (either magnetic or nonmagnetic) induced by magnetic field gradients is given by (Jones 1995; Pamme 2006; Suwa and Watarai 2011):

$$\begin{aligned}\mathbf{F}_m &= 3\mu_0 V_p \frac{\chi_p - \chi_f}{3 + \chi_p + 2\chi_f}(\mathbf{H}\bullet\nabla)\mathbf{H} \\ &\cong \mu_0 V_p(\chi_p - \chi_f)(\mathbf{H}\bullet\nabla)\mathbf{H}\end{aligned} \quad (1)$$

where $\mu_0 = 4\pi \times 10^{-7}$ H/m is the permeability of free space, V_p is the volume of the particle, χ_p is the magnetic susceptibility of the particle, χ_f is the magnetic susceptibility of the suspending fluid, and $\mathbf{H}$ is the magnetic field at the particle center. The formula after the second equal sign is valid with negligible errors because both χ_p and χ_f are at least three orders of magnitude smaller than 1 for the nonmagnetic particles and paramagnetic solutions used in this study. Moreover, as $\chi_p < \chi_f$, nonmagnetic particles suspended in paramagnetic solutions are directed by $\mathbf{F}_m$ against the magnetic field gradient, i.e., along the direction of decreasing magnetic field magnitude. For a rectangular permanent magnet with magnetization along the z direction, the analytical formulae for the three components of $\mathbf{H}$, i.e., H_x, H_y and H_z, are given by (Furlani 2001):

$$\begin{aligned}H_x(x,y,z) = &\frac{M_s}{4\pi}\sum_{i=1}^{2}\sum_{j=1}^{2}(-1)^{i+j}\ln \\ &\times\left\{\frac{(y-y_1)+\left[(x-x_i)^2+(y-y_1)^2+(z-z_j)^2\right]^{1/2}}{(y-y_2)+\left[(x-x_i)^2+(y-y_2)^2+(z-z_j)^2\right]^{1/2}}\right\}\end{aligned} \quad (2)$$

$$\begin{aligned}H_y(x,y,z) = &\frac{M_s}{4\pi}\sum_{i=1}^{2}\sum_{j=1}^{2}(-1)^{i+j}\ln \\ &\times\left\{\frac{(x-x_1)+\left[(x-x_1)^2+(y-y_i)^2+(z-z_j)^2\right]^{1/2}}{(x-x_2)+\left[(x-x_2)^2+(y-y_i)^2+(z-z_j)^2\right]^{1/2}}\right\}\end{aligned} \quad (3)$$

$$\begin{aligned}H_z(x,y,z) = &\frac{M_s}{4\pi}\sum_{i=1}^{2}\sum_{j=1}^{2}\sum_{k=1}^{2}(-1)^{i+j+k}\tan^{-1} \\ &\times\left\{\frac{(x-x_i)(y-y_j)}{(z-z_k)\left[(x-x_i)^2+(y-y_j)^2+(z-z_k)^2\right]^{1/2}}\right\}\end{aligned} \quad (4)$$

where the coordinate system originates from the center of the magnet, and $M_s = 1.05 \times 10^6$ A/m is the residual magnetization of the permanent magnet as calculated from the residual magnetic flux density, B_s (=1.32 T as per the manufacturer), through $M_s = B_s/\mu_0$. Other symbols involved in the magnetic field equations are $x_1 = x_m$, $x_2 = -x_m$, $y_1 = y_m, y_2 = -y_m, z_1 = z_m$, and $z_2 = -z_m$ with x_m, y_m, and z_m being one half of the dimensions of the magnet in the x, y, and z directions, respectively.

The total magnetic field of the two stacked permanent magnets in Fig. 1 is simply the superposition of $\mathbf{H}$ of each magnet given in Eqs. 2–4. Fig. 2 shows the contours of the total magnetic field magnitude in the horizontal (at $y = -y_m + h_c/2$ with h_c being the microchannel height, left plot) and vertical (at $x = 0$, right plot) planes of the microchannel. Table 1 summarizes the parameters involved in the calculation. It is evident that the magnets generate strong magnetic field gradients nearby in all the three directions. Moreover, the further away from the center of the magnets, the smaller the local magnetic field is. Therefore, nonmagnetic particles should be deviated from the fluid flow in the x-direction, and be deflected

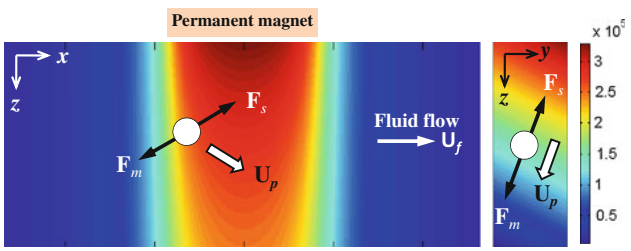

Fig. 2 Force analyses on a nonmagnetic particle suspended in $MnCl_2$ solution in the horizontal (*left plot*) and vertical (*right plot*) planes of a microchannel. The background shows the contours of magnetic field strength (in the unit of H/m) in the absence of the nonmagnetic particle. $\mathbf{F}_m$ and $\mathbf{F}_s$ denote the magnetic and Stokes drag forces, respectively. $\mathbf{U}_f$ and $\mathbf{U}_p$ denote the fluid and particle velocities, respectively. The microchannel and magnet are not drawn to scale

Table 1 List of the parameters used in the analytical model

Parameter		Description	Value	Unit
Magnet	M_s	Residual magnetization	1.05×10^6	A/m
	$2x_m$	Length	3.176	mm
	$2y_m$	Height	3.176	mm
	$2z_m$	Thickness (polar direction)	1.588	mm
		Magnets-channel distance	260	μm
$MnCl_2$ solution	c	Molar concentration	40, 200, 1000	mM
	ρ_f	Mass density	1050	kg/m^3
	η_f	Dynamic viscosity	1×10^{-3}	kg/m/s
	χ_f	Magnetic susceptibility	Eq. (9)	
Nonmagnetic particles	d	Particle diameter	5, 10, 15	μm
	χ_p	Magnetic susceptibility	-5×10^{-6}	
	l_c	Channel length	2	cm
Microchannel	w_c	Channel width	200	μm
	h_c	Channel height	25	μm
	U_{avg}	Average flow speed	200, 400, 600	μm/s

along both the positive z and negative y directions as illustrated by the force analyses in Fig. 2. The result is a three-dimensionally focused particle stream flowing near the outer bottom corner of the microchannel. However, since the depth (25 μm) of the current channel is much smaller than its width (200 μm), particles are expected to be deflected toward the bottom wall much more quickly than to the outer sidewall. Therefore, for simplicity, we assume in our model (see Sect. 3.2 for detail) that particles are brought into touch with the bottom wall momentarily by the vertical magnetic force and then move through the magnets region only in the horizontal plane.

The particle *deflection* in the horizontal plane (i.e., x–z plane) of the microchannel is determined by the ratio of the particle velocities, $\mathbf{U}_p$, perpendicular and parallel to the flow,

$$\text{Deflection} = \frac{U_{p,z}}{U_{p,x}} = \frac{U_{m,z}}{U_f + U_{m,x}} \tag{5}$$

where U_f is the axial flow velocity (White 1991)

$$U_f = \frac{\pi U_{avg}}{2}\left\{\left[1 - \frac{\cosh\left(\frac{\pi z'}{h_c}\right)}{\cosh\left(\frac{\pi w_c}{2h_c}\right)}\right]\cos\left(\frac{\pi y'}{h_c}\right) - \frac{1}{27}\left[1 - \frac{\cosh\left(\frac{3\pi z'}{h_c}\right)}{\cosh\left(\frac{3\pi w_c}{2h_c}\right)}\right]\cos\left(\frac{3\pi y'}{h_c}\right)\right\} \left\{\left[1 - \frac{2h_c}{\pi w_c}\tanh\left(\frac{\pi w_c}{2h_c}\right)\right] - \frac{1}{81}\left[1 - \frac{2h_c}{3\pi w_c}\tanh\left(\frac{3\pi w_c}{2h_c}\right)\right]\right\}^{-1} \tag{6}$$

with U_{avg} being its cross-sectional area-average

$$U_{avg} = \frac{\rho_f g \Delta h}{l_c}\frac{8h_c^2}{\eta_f \pi^4}\left\{\left[1 - \frac{2h_c}{\pi w_c}\tanh\left(\frac{\pi w_c}{2h_c}\right)\right] - \frac{1}{81}\left[1 - \frac{2h_c}{3\pi w_c}\tanh\left(\frac{3\pi w_c}{2h_c}\right)\right]\right\} \tag{7}$$

In the last two equations, ρ_f is the density of the $MnCl_2$ solution, g is the gravitational acceleration, Δh is the liquid height difference in the upstream and downstream reservoirs of the microchannel that provides the pressure-drop for driving the particle suspension, l_c, h_c, and w_c are the length, height, and width of the microchannel, and η_f the dynamic viscosity of the suspending solution. The auxiliary coordinates y' and z' in Eq. 6 originate from the center of the channel cross-section and are parallel to the y and z coordinates for the magnet (see Fig. 1), respectively.

The magnetophoretic particle velocity, $\mathbf{U}_m$, in Eq. 5 can be obtained by balancing the magnetic force, $\mathbf{F}_m$, in Eq. 1 with the Stokes drag force (see $\mathbf{F}_s$ in Fig. 2),

$$\mathbf{U}_m = \frac{\mathbf{F}_m}{3\pi\eta_f d f_D} = \frac{\mu_0 d^2(\chi_p - \chi_f)(\mathbf{H}\bullet\nabla)\mathbf{H}}{18\eta_f f_D} \quad (8)$$

where d is the particle diameter, and $f_D = 3.1$ is the drag coefficient accounting for the channel wall's retardation effect on particle motion (Happel and Brenner 1973). The magnetic susceptibility of the $MnCl_2$ solution is assumed to increase linearly with the concentration of $MnCl_2$, c, via (Mirica et al. 2009).

$$\chi_f = 1.877 \times 10^{-4} c - 9 \times 10^{-6} \quad (9)$$

Therefore, $\mathbf{U}_m$ and hence the particle *deflection* should increase with increasing particle size and $MnCl_2$ concentration. In addition, lowering the flow velocity should also enhance the particle deflection according to Eq. 5.

3.2 Simulation of particle trajectory

We developed an analytical model to simulate the trajectory of nonmagnetic particles in paramagnetic solutions in response to magnetic field gradients. As explained earlier, this model assumes that particles are in touch with the bottom wall of the microchannel and travel only in the horizontal plane (i.e., x–z plane) for simplicity. The instantaneous position of a particle, $\mathbf{r}_p$, was obtained by integrating the particle velocity over time,

$$\mathbf{r}_p = \mathbf{r}_0 + \int_0^t [\mathbf{U}_f(t') + \mathbf{U}_m(t')]dt' \quad (10)$$

where $\mathbf{r}_0$ is the initial location of the particle, and t is the time coordinate. It is noted that both the fluid velocity, $\mathbf{U}_f$, and the magnetophoretic particle velocity, $\mathbf{U}_m$, are dependent on position, and so vary with time during the particle migration. Inertia is neglected in Eq. 10 as both the calculated fluid and particle Reynolds numbers are much smaller than 1 in the experimental conditions (Di Carlo et al. 2007). A custom-written Matlab® program was employed to determine the particle position with respect to time and to plot the particle trajectory. A total of twenty evenly distributed points over the width were picked at the entrance of the microchannel as the initial particle positions. The magnetic field components were calculated from Eqs. 2–4 by setting $y = -y_m + d/2$, i.e., the y-coordinate value of the particle center. This same y value was also assigned to Eq. 6 to determine the axial fluid velocity U_f. All the parameters involved in the model are listed in Table 1 unless otherwise stated in the text.

4 Results and discussion

4.1 Evolution of horizontal particle deflection

To understand how the magnetic deflection evolves when particles approach and move by the permanent magnets, we studied 10 μm particle motions in 1 M $MnCl_2$ solution through a row of five observation windows along the channel length. The relative positions of these windows with respect to the magnets are 0.5 mm upstream (Window 1), align with the front edge (Window 2), center (Window 3), align with the back edge (Window 4), and 0.5 mm downstream (Window 5). Figure 3a shows the top-view images (top row for snapshot, bottom row for superimposed) in the five observation windows at an average flow speed of $U_{avg} = 800$ μm/s. One can see that particles follow the fluid flow in Window 1, indicating negligible magnetic force when particles are 0.5 mm ahead of the magnets. When they approach the front edge of the magnets in Window 2, particles start being deviated from the axial flow direction and acquire a noticeable deflection away from the magnets. This horizontal deflection grows continuously to nearly the entire channel width as particles move through the magnets region, which is clear from the images in Windows 2–4. It vanishes when particles move into Window 5. Therefore, the effective region for particle magnetophoresis is restricted to only the part of the microchannel that is right beside the magnets.

The observed lengthwise evolution of particle deflection in Fig. 3a is accurately predicted by the analytical model as demonstrated in Fig. 3b, where the experimentally measured (symbols, determined from the superimposed images) and theoretically predicted (curve) widths of the focused particle stream are quantitatively compared. The experimental error in measuring the stream width is less than 10 μm, which is too small to be clearly illustrated in Fig. 3b and thus, not included. A good agreement is observed for the results in all the five observation windows. Moreover, the inset images in Fig. 3b demonstrate that in Window 1 particles appear in different brightness and thus should stay in different focal planes, i.e., different vertical planes of the microchannel. In contrast, all the particles in Window 5 exhibit a nearly identical appearance and, are thus, within the same focal plane. This indicates a three-dimensional focusing effect due to the horizontal and vertical magnetophoretic deflections as noted in the Theory section (see also Fig. 2).

The observation in Fig. 3 is also consistent with the axial distribution of the predicted magnetophoretic particle velocity, $\mathbf{U}_m$, along the channel centerline. As seen in Fig. 4, the cross-stream component, U_{mz}, acquires a positive value (on the order of 10 μm/s) only within

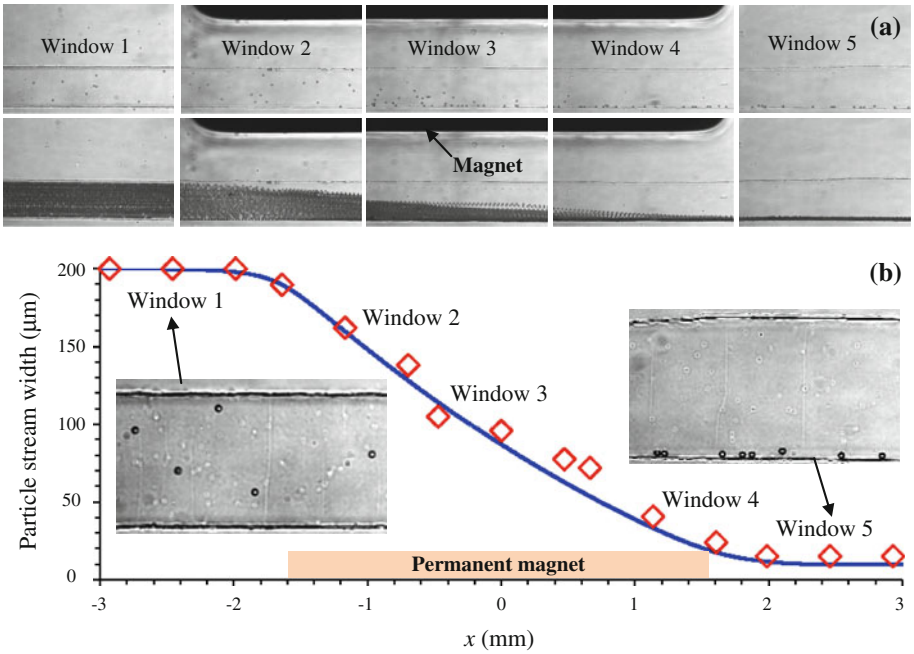

Fig. 3 Lengthwise evolution of the magnetophoretic deflection of 10 μm polystyrene particles suspended in 1 M $MnCl_2$ solution at an average flow speed of 800 μm/s: snapshot (*top row*) and superimposed (*bottom row*) images in the five consecutive observation windows along the channel length (**a**); comparison of the experimentally measured (symbols) and theoretically predicted (*curve*) widths of the particle stream along the flow direction (**b**). The *insets* of (**b**) show the magnified images of particles in Windows 1 and 5, respectively. The position of the two stacked permanent magnets is indicated in the superimposed image in Window 3 of (**a**) and is also highlighted in (**b**)

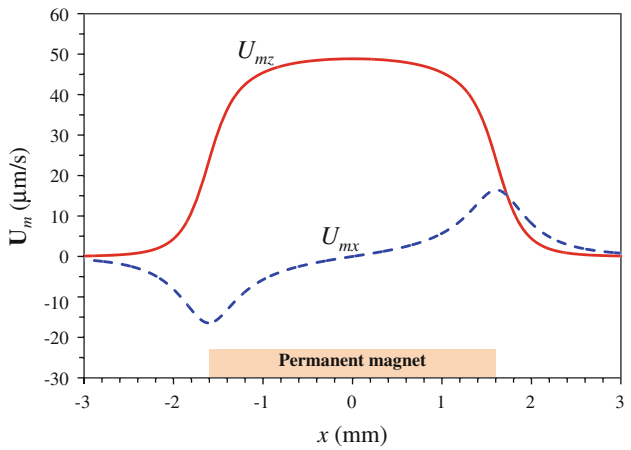

Fig. 4 Axial distribution of the theoretically predicted magnetophoretic particle velocity, $\mathbf{U}_m$, along the centerline of the microchannel. All the conditions are referred to Fig. 3

0.5 mm distance before and after the magnet (i.e., -2 mm $< x < +2$ mm), which explains the question of why no apparent particle deflection is observed in Windows 1 and 5 of Fig. 3. The streamwise magnetophoretic velocity, U_{mx}, also obtains a non-zero value in the same range of x as U_{mz} though at a smaller magnitude. Moreover, U_{mx} varies from negative in the upstream half of the magnet, which hinders the particle motion, to positive in the downstream half, which propels the particle.

4.2 Particle size effect on particle deflection

Equation 8 indicates that the magnetophoretic velocity is proportional to particle diameter squared. As a result, the magnetic deflection should be a quadratic function of particle diameter, if the fluid velocity is much greater than the axial magnetophoretic particle velocity, i.e., $U_f >> U_{m,x}$ in Eq. 5. This condition is fulfilled in our experiment as $U_{m,x}$ is on the order of 10 μm/s, while the lowest flow velocity we used is 200 μm/s. Figure 5 shows the experimentally obtained images (left column for snapshot, middle column for superimposed) and theoretically predicted trajectories (right column) of 5-, 10-, and 15-μm-diameter particles in Windows 2 (a) and 5 (b) of the magnets-microchannel system (see Fig. 3 for the locations of the observation windows). The average flow speed of the particle suspensions in 200 mM $MnCl_2$ solution is 200 μm/s. It is evident from the images that larger particles acquire a greater deflection in both the observation windows, which agree reasonably with the theoretical predictions for all the particle sizes.

Figure 6 shows a quantitative comparison of the experimentally measured (symbols, see also the inset images) and theoretically predicted (curved) stream widths of different particles 0.5 mm after the magnets (i.e., in observation Window 5). It is noted that the horizontal axis is the particle diameter squared. The agreement is good for all the three particle sizes. Moreover, the stream widths of 5 and 10 μm particles indeed approximately scale with the square of their diameters. The deviation from the second order dependence for particles smaller than 5 μm particles is probably attributed to the variation of the magnetic field and fluid velocity at the particle center with particle size. For particles larger than 14 μm, the model predicts a full-width deflection and so the particle stream width becomes essentially equal to the particle diameter. This prediction is

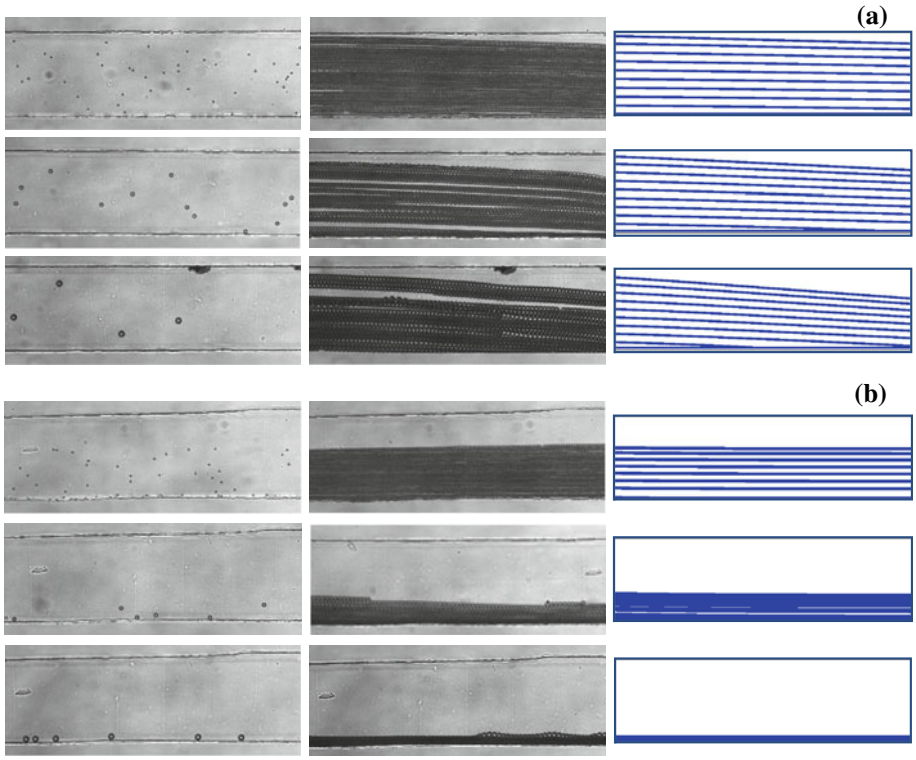

Fig. 5 Illustration of particle size effect on the deflection of nonmagnetic particles in Window 2 (**a**) and Window 5 (**b**) of the magnets-microchannel system (see Fig. 3 for the locations of the observation windows), where the *top*, *middle,* and *bottom* rows in each panel are for particles of 5, 10, and 15 μm in diameter, respectively. The columns from *left* to *right* show the snapshot image, superimposed image, and theoretically predicted trajectories of the particles, respectively. All the particles were re-suspended in 200 mM $MnCl_2$ solution. The average flow speed was fixed at 200 μm/s

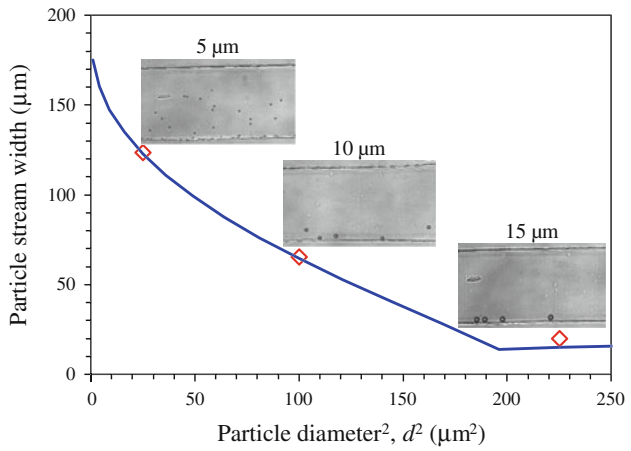

Fig. 6 Particle size effect on the magnetic deflection in 200 mM $MnCl_2$ solution at a fixed flow speed of 200 μm/s. The *symbols* represent the experimental data of particle stream width 0.5 mm after the magnets (see also the *inset* snapshot images). The curve is obtained from the analytical model

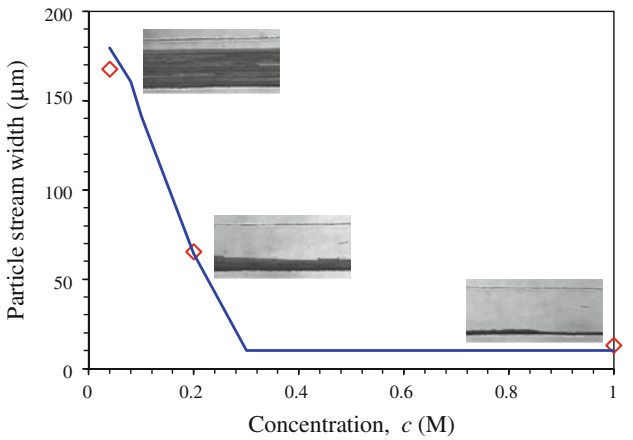

Fig. 7 $MnCl_2$ concentration effect on the deflection of 10 μm nonmagnetic particles at an average flow speed of 200 μm/s. The *symbols* represent the experimental data of particle stream width measured from the corresponding superimposed images. The curve is obtained from the analytical model

evidenced from the inset image in Fig. 6, where 15 μm particles all line the channel sidewall as a consequence of the negative magnetophoretic deflection.

4.3 $MnCl_2$ concentration effect on particle deflection

The molar concentration of $MnCl_2$ salt, c, affects the magnetic susceptibility, χ_f, density, ρ_f, and viscosity, η_f, of the solution, among which the changes in the latter two properties are much smaller than that in χ_f. Therefore, we neglected the $MnCl_2$ concentration effects on the fluid density and viscosity in the analytical model. The magnetophoretic particle deflection is expected to be linearly proportional to c. This analysis is verified in Fig. 7, where the experimentally measured stream widths of 10 μm particles suspended in 40 mM, 200 mM, and 1 M $MnCl_2$ solutions (symbols, see also the inset superimposed images) closely match the theoretical prediction (curve). The

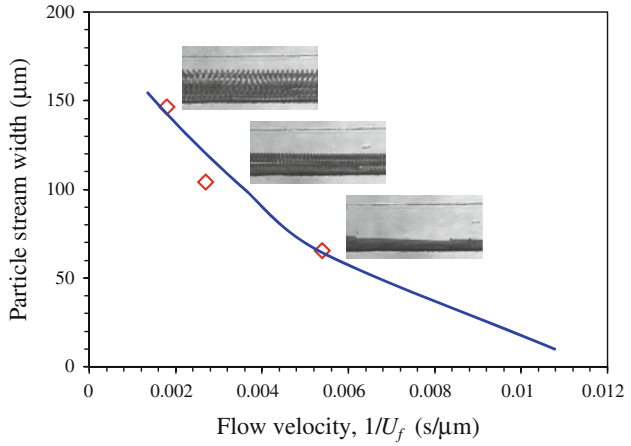

Fig. 8 Flow velocity effect on the deflection of 10 μm nonmagnetic particles suspended in 200 mM $MnCl_2$ solution. The *symbols* represent the experimental data of particle stream width measured from the corresponding superimposed images. The curve is obtained from the analytical model

model predicts that 10 μm particles should achieve a full-width deflection when the $MnCl_2$ concentration is larger than 300 mM, which is supported by the experimental data at 1 M concentration. Below 300 mM, the particle stream width decreases (equivalently, particle deflection increases) linearly with the $MnCl_2$ concentration as expected.

4.4 Flow effect on particle deflection

Equation 5 indicates that particle deflection should decrease linearly with increasing flow speed of the $MnCl_2$ solution as long as $U_f >> U_{m,x}$. To test this, we studied the deflection of 10 μm particles in 200 mM $MnCl_2$ solution when the average flow speed was varied from 200 to 600 μm/s. The experimental results (symbols and inset images) of the particle stream width are compared with the theoretical prediction (curve) in Fig. 8, where a reasonable agreement is found for the three tested flow velocities. It is noted that the horizontal axis is the inverse of the flow velocity. We see that to a good approximation, the predicted particle stream width is inversely proportional to the flow velocity, which is consistent with the experimental results.

5 Conclusion

We have developed a method to embed permanent magnets into PDMS, and demonstrated that the magnet-microchannel distance can be precisely controlled down to 260 μm. This enables a continuous-flow manipulation of nonmagnetic microparticles in paramagnetic solutions on PDMS-based microfluidic chips. We have performed combined experimental and theoretical studies of polystyrene particle motion in $MnCl_2$ solutions through an on-chip rectangular microchannel. It is found that particles are pushed away from the magnets both horizontally and vertically, forming a focused particle stream flowing near the outer bottom corner of the microchannel. The horizontal deflection grows continuously as particles move by the magnets, where the effective working range is within only the channel region right besides the magnets. The overall particle deflection after the magnets, if not fully deflected, has been observed to increase approximately linear with the particle diameter squared, the $MnCl_2$ concentration, and the inverse of the flow velocity. These relationships have been verified in our experiment, which agree quantitatively with the predictions of an analytical model.

Acknowledgments This study was partially supported by Clemson University through a start-up package.

References

Ando B, Baglio S, Beninato A (2010) Magnetic fluids for bio-medical application. In: Lecture notes in electrical engineering, vol 55, pp 16–28

Annavarapu VNR (2010) Size based separation of submicron nonmagnetic particles through magnetophoresis in structured obstacle arrays, MIT, PhD dissertation

Di Carlo D, Irimia D, Tompkins RG, Toner M (2007) Continuous inertial focusing, ordering, and separation of particles in microchannels. Proc Natl Acad Sci USA 104:18892–18897

Erb RM, Yellen BB (2008) Concentration gradients in mixed magnetic and nonmagnetic colloidal suspensions. J Appl Phys 103:07A312

Erb RM, Yellen BB (2009) Magnetic manipulation of colloidal particles. In: Liu JP (ed) Nanoscale magnetic materials and applications. Springer, New York, pp 563–590

Erb RM, Son HS, Samanta B, Rotello VM, Yellen BB (2009) Magnetic assembly of colloidal superstructures with multipole symmetry. Nature 457:999–1002

Fateen SK (2002) Magnetophoretic focusing of submicron particles dispersed in a polymer-stabilized magnetic fluid, MIT, PhD dissertation

Feinstein E, Prentiss M (2006) Three-dimensional self-assembly of structures using the pressure due to a ferrofluid in a magnetic field gradient. J Appl Phys 99:064901

Friedman G, Yellen B (2005) Magnetic separation, manipulation, and assembly of solid phase in fluids. Current Opinion Colloid Inters Sci 10:158–166

Furlani EP (2001) Permanent magnet and electromechanical devices: materials. analysis, and applications. Academic Press, San Diego

Gijs MAM (2004) Magnetic bead handling on-chip: new opportunities for analytical applications. Microfluid Nanofluid 1:22–40

Gijs MAM, Lacharme F, Lehmann U (2010) Microfluidic applications of magnetic particles for biological analysis and catalysis. Chem Rev 110:1518–1563

Hahn YK, Park JK (2011) Versatile immunoassays based on isomagnetophoresis. Lab Chip. (in press). doi: 10.1039/C0LC00569J

Halverson D, Kalghatgi S, Yellen B, Friedman G (2006) Manipulation of nonmagnetic nanobeads in dilute ferrofluid. J Appl Phys 99:08P504

Han KH, Frazier AB (2006) Paramagnetic capture mode magnetophoretic microseparator for high efficiency blood cell separations. Lab Chip 6:265–273

Happel J, Brenner H (1973) Low Reynolds number hydrodynamics. Springer, London

Jones TB (1995) Electromechanics of particles. Cambridge University Press, New York

Jung YD, Choi Y, Han KH, Fraizer AB (2010) Six-stage cascade paramagnetic mode magnetophoretic separation system for human blood samples. Biomed Microdev 12:637–645

Kang JH, Choi S, Lee W, Park JK (2008) Isomagnetophoresis to discriminate subtle difference in magnetic susceptibility. J Am Chem Soc 130:396–397

Kirby BJ (2010) Micro- and nanoscale fluid mechanics: transport in microfluidic devices. Cambridge University Press, Cambridge

Kose AR, Fischer B, Mao L, Koser H (2009) Label-free cellular manipulation and sorting via biocompatible ferrofluids. Proc Natl Acad Sci USA 106(51):21478–21483

Krebs MD, Erb RM, Yellen BB, Samanta B, Bajaj A, Rotello VM, Alsberg E (2009) Formation of ordered cellular structures in suspension via label-free negative magnetophoresis. Nano Lett 9:1812–1817

Li KH, Yellen BB (2010) Magnetically tunable self-assembly of colloidal rings. Appl Phys Lett 97:083105

Liu CX, Stakenborg T, Peeters S, Lagae L (2009) Cell manipulation with magnetic particles toward microfluidic cytometry. J Appl Phys 105:102011–102014

Mirica KA, Phillips ST, Shevkoplyas SS, Whitesides GM (2009) Measuring densities of solids and liquids using magnetic levitation: Fundamentals. J Am Chem Soc 131:10049–10058

Pamme N (2006) Magnetism and microfluidics. Lab Chip 6:24–38

Pamme N, Manz A (2004) On-chip free-flow magnetophoresis: Continuous flow separation of magnetic particles and agglomerates. Anal Chem 76:7250–7256

Pamme N, Wilhelm C (2006) Continuous sorting of magnetic cells via on-chip free-flow magnetophoresis. Lab Chip 6:974–980

Peyman SA, Kwan EY, Margarson O, Iles A, Pamme N (2009) Diamagnetic repulsion—a versatile tool for label-free particle handling in microfluidic devices. J Chromatogr A 1216:9055–9062

Pohl HA (1978) Dielectrophoresis. Cambridge University Press, Cambridge

Rodriguez-Villarreal AI, Tarn MD, Madden LA, Lutz JB, Greenman J, Samitier J, Pamme N (2011) Flow focusing of particles and cells based on their intrinsic properties using a simple diamagnetic repulsion setup. Lab Chip 11:1240–1248

Rosensweig RE (1985) Ferrohydrodynamics. Cambridge University Press, Cambridge

Rosensweig RE (1987) Magnetic fluids. Annu Rev Fluid Mech 19: 437–463

Sharpe SA (2004) Magnetophoretic cell clarification, MIT, PhD dissertation

Suwa M, Watarai H (2011) Magnetoanalysis of micro/nanoparticles: a review. Anal Chimica Acta 690:137–147

Tarn MD, Hirota N, Hes A, Pamme N (2009) On-chip diamagnetic repulsion in continuous flow. Sci Technol Adv Mater 10:014611

Watarai H, Namba M (2001) Magnetophoretic behavior of single polystyrene particles in aqueous manganese(II) chloride. Anal Sci 17:1233–1236

Watarai H, Namba M (2002) Capillary magnetophoresis of human blood cells and their magnetophoretic trapping in a flow system. J Chromatogr A 961:3–8

Watarai H, Suwa M, Iiguni Y (2004) Magnetophoresis and electromagnetophoresis of microparticles in liquids. Anal Bioanal Chem 378:1693–1699

White FM (1991) Viscous fluid flow. McGraw-Hill Science/Engineering/Math, New York

Winkleman A, Gudiksen KL, Ryan D, Whitesides GM (2004) A magnetic trap for living cells suspended in a paramagnetic buffer. Appl Phys Lett 85:2411–2413

Yellen BB, Friedman G (2004) Programmable assembly of colloidal particles using magnetic microwell templates. Langmuir 20: 2553–2559

Yellen BB, Friedman G, Feinerman A (2003) Printing superparamagnetic colloidal particle arrays on patterned magnetic film. J Appl Phys 93:7331–7333

Yellen BB, Hovorka O, Friedman G (2005) Arranging matter by magnetic nanoparticle assemblers. Proc Natl Acad Sci USA 102:8860–8864

Zhu J, Tzeng TJ, Hu G, Xuan X (2009) Dielectrophoretic focusing of particles in a serpentine microchannel. Microfluid Nanofluid 7: 751–756

Zhu TT, Marrero F, Mao LD (2010) Continuous separation of non-magnetic particles inside ferrofluids. Microfluid Nanofluid 9: 1003–1009

Zhu TT, Lichlyter DJ, Haidekker MA, Mao L (2011) Analytical model of microfluidic transport of non-magnetic particles in ferrofluids under the influence of a permanent magnet. Microfluid Nanofluid 10:1233–1245